

Elucidating the Electrochemical Behaviour of a P3-type High Na Content Cathode

Samriddhi Saxena, Manish Badole, Hari Narayanan Vasavan, Velaga Srihari, Asish Kumar Das, Pratiksha Gami, Neha Dagar, Sonia Deswal, Pradeep Kumar, Himanshu Kumar Poswal, Sunil Kumar*

Abstract

Layered oxide materials are often regarded as prospective positive electrodes for Na-ion batteries owing to their superior electrochemical properties and facile synthesis. In this work, a high-Na content P3-type cathode ($\text{NaMn}_{0.6}\text{Ni}_{0.3}\text{Cu}_{0.1}\text{O}_2$; P3-NMNC) was prepared by the sol-gel technique. These materials exhibited excellent rate performance and specific capacity (discharge specific capacity at 3C being 77% of that at 0.1C). Even at 10C, the cells retained $\sim 45 \text{ mAh g}^{-1}$. The P3-NMNC half-cells were cycled between two voltage ranges, 2.0 – 4.0 V and 2.0 – 4.2 V, among which the former exhibited an 83% capacity retention after 200 cycles, which was vastly superior to the latter, where the degradation in the capacity dropped below 80% in just 75 cycles. The dQ/dV vs. V plots revealed an irreversible peak above 4.0 V during the first desodiation process, which is attributed to an irreversible anionic redox leading to poor cyclability. *Operando* Synchrotron X-ray diffraction studies revealed a reversible $\text{P3} \leftrightarrow \text{P3}' \leftrightarrow \text{O3}$ transformation in NMNC during sodiation-desodiation. The repeated $\text{P3}' \leftrightarrow \text{O3}$ transformations resulted in strain due to changes in lattice parameters causing capacity degradation. The D_{Na^+} was determined using the galvanostatic intermittent titration technique in the order of 10^{-12} to $10^{-10} \text{ cm}^2 \text{ s}^{-1}$. These results underscore the importance of the scarcely explored high Na-content P3-type layered oxide cathodes towards the advancement of Na-ion batteries.

Keywords: *P3-type cathode, Na-ion batteries, Cycle life, Operando Synchrotron XRD, Phase transformation.*

1. INTRODUCTION

Lithium-ion batteries (LIBs) are highly sought after as energy storage solutions across various applications, including power electronics and electric vehicles, owing to their impressive energy density. However, the rapid adoption of LIB technology raises concerns about the availability of essential metals such as Li and Co for fabricating LIB cells.^{1, 2} Given their lower cost and abundance of sodium deposits, Na-ion batteries (NIBs) have emerged as a viable replacement for LIBs.³⁻⁶ As cathode material contributes largely towards the energy density of cells significant efforts are made to explore optimal cathode materials that exhibit better electrochemical performance.⁷⁻¹²

Sodium-based layered oxides (Na_xTMO_2) stand out as a highly promising and versatile group of materials as positive electrodes in NIBs. Here, TM denotes one or more redox-active 3d transition metals and smaller amounts of redox-inactive elements like Mg or Al, typically incorporated to fine-tune material properties.¹³⁻¹⁷ The structural configuration of these materials is primarily governed by the interlayer electrostatic repulsion between TM-O₆ and Na-O₆ units. Na_xTMO_2 layered oxides are classified into four distinct categories: O2, O3, P2, and P3. This is based on the coordination environment of Na ions (P stands for prismatic, and O denotes octahedral) and the number of repeating TM layers in one unit cell.^{18, 19}

P2-type $\text{Na}_{0.67}\text{Ni}_{0.33}\text{Mn}_{0.67}\text{O}_2$ and O3-type $\text{NaNi}_{0.5}\text{Mn}_{0.5}\text{O}_2$ are among the various extensively studied layered oxide materials. The P2 phase is recognized for its superior rate capability over the O3 phase due to its more open framework. Since the cathode acts as the source of Na-ions during full-cell operation, the adoption of P2-type materials in full cells is hampered by their limited Na content. On the other hand, O3-type $\text{NaNi}_{0.5}\text{Mn}_{0.5}\text{O}_2$ have a higher Na

content and are hence feasible for practical applications. However, they suffer from slow Na^+ diffusion and poor cyclic performance, especially at voltages beyond 4 V.²⁰⁻²⁷

Recently, considerable research has focused on the P3-type layered oxides as potential cathodes for NIBs because of their high discharge capacity and relatively simple synthesis process.²⁸⁻³⁰ For instance, Guo et al. synthesized a P3-type $\text{Na}_{0.63}\text{Ti}_{0.37}\text{Cr}_{0.63}\text{O}_2$ cathode, which reportedly retained 84% of its initial specific capacity (82 mAh g^{-1}) after 400 cycles at 1C. However, the study also highlights the consequence of the low Na content in layered oxide materials which led to a low specific discharge capacity in the $\text{Na}_{0.63}\text{Ti}_{0.37}\text{Cr}_{0.63}\text{O}_2$ cathode.³¹ Several other strategies have also been explored to enhance the electrochemical properties of P3-type cathodes such as utilizing a reversible lattice oxygen redox along with $\text{Mn}^{3+}/\text{Mn}^{4+}$ redox reaction to deliver a higher discharge capacity.³² In a different study, Hou et al. designed a compositionally graded P3-type $\text{Na}_{0.5}[\text{Ni}_{0.216}\text{Mn}_{0.784}]\text{O}_2$ cathode material exhibiting specific capacities as high as 164.5 mAh g^{-1} at 0.1C while retaining 72.9% after 400 cycles at 1C.³³ Zou et al. have shown that the utilization of ClO_4^- anion present in the electrolyte in the electrochemical processes leads to a notable enhancement in the electrochemical performance of P3- $\text{Na}_{0.5}\text{Ni}_{0.25}\text{Mn}_{0.75}\text{O}_2$.³⁴ The development of multiphasic P3-based materials has further improved the electrochemical properties of NIB cathodes.³⁵⁻³⁹ Nevertheless, it is crucial to further enhance the specific capacities of these materials with low initial Na content. P3-type cathodes with increased Na content have been reported by adjusting their composition. Risthaus et al. reported a P3 type $\text{Na}_{0.9}\text{Ni}_{0.5}\text{Mn}_{0.5}\text{O}_2$ cathode with a high Na content exhibiting 140 mAh g^{-1} at 0.1C. A lowered Na^+ diffusion barrier between trigonal prismatic Na sites resulted in high cycle stability and rate capability, making it more suitable for practical applications.⁴⁰ Other studies have reported higher specific capacities in P3- $\text{Na}_{0.9}\text{Fe}_{0.5}\text{Mn}_{0.5}\text{O}_2$ ⁴¹, P3- $\text{Na}_{0.75}\text{Mg}_{0.08}\text{Co}_{0.10}\text{Ni}_{0.2}\text{Mn}_{0.60}\text{O}_2$ ⁴², and $\text{Na}_{0.6}\text{Ni}_{0.3}\text{Mn}_{0.7}\text{O}_2$ ⁴³.

This study reports the electrochemical properties of a monophasic high Na content P3-type $\text{NaMn}_{0.6}\text{Ni}_{0.3}\text{Cu}_{0.1}\text{O}_2$ (P3-NMNC) cathode material. Manganese and nickel-based materials typically exhibit superior specific discharge capacity and rate capability, rendering them as attractive candidates for cathode material selection.^{21, 25} The $\text{Ni}^{2+}/\text{Ni}^{4+}$ redox process demonstrates significant specific capacity, while the electrochemically inert Mn^{4+} contributes to structural stability. Additionally, incorporating copper ions within the TM layers makes the layered oxides moisture stable and enhances their nominal voltage and cyclability. Recent progress in the $\text{Na}_x(\text{Mn-Ni-Cu})\text{O}_2$ based layered oxides has showcased $\sim 120 \text{ mAh g}^{-1}$ with a nominal voltage of around 3.4 V and an impressive cyclability after 500 cycles at 1C.⁴⁴⁻⁴⁷ A systematic evaluation of the electrochemical properties of P3-NMNC in different voltage ranges demonstrates better cyclic stability in the 2.0 – 4.0 V range compared to the 2.0 – 4.2 V range. The correlation between cyclability and structural changes of the P3-NMNC are further investigated by *operando* Synchrotron X-ray diffraction (SXRD) measurements, which reveal a $\text{P3} \leftrightarrow \text{P3}' \leftrightarrow \text{O3}$ transformation during charge/discharge. These findings demonstrate the potential of the P3 phase with high Na content in driving the advancement of layered oxides for sodium-ion batteries.

2. MATERIALS AND METHODS

2.1. Material Synthesis

The $\text{NaMn}_{0.6}\text{Ni}_{0.3}\text{Cu}_{0.1}\text{O}_2$ with P3 phase structure was prepared *via* a conventional sol-gel method. Na_2CO_3 (SRL, 99.9%), $\text{C}_4\text{H}_6\text{MnO}_4 \cdot 4\text{H}_2\text{O}$ (Sigma Aldrich, > 99%), $\text{C}_4\text{H}_6\text{NiO}_4 \cdot 4\text{H}_2\text{O}$ (Sigma Aldrich, 98%), and $\text{Cu}(\text{NO}_3)_2 \cdot 3\text{H}_2\text{O}$ (Thermo Fisher, 99%) were dissolved in deionized water along with appropriate amounts of $\text{C}_6\text{H}_8\text{O}_7$ (citric acid) and $\text{C}_2\text{H}_6\text{O}_2$ (ethylene glycol). The solution was heated to obtain gel, which was dried and heat treated at 550 °C. The resulting powder was calcined in air at 700 °C to produce the required product.

2.2. Structural Characterization

Inductively coupled plasma mass spectrometry (ICP-MS) was performed using an Agilent Model- 7850 LC-ICP-MS. X-ray diffraction (XRD) data was obtained from an Empyrean diffractometer (Malvern Panalytical), utilizing Cu-K α radiation. The diffraction data was analyzed using TOPAS Academic (version 6) software to calculate the crystallographic parameters.⁴⁸ The crystallographic structure of the cathode materials was studied using X-ray absorption fine structure spectroscopy (EXAFS), which was carried out at the Indus-2 synchrotron source at the Raja Ramanna Centre for Advanced Technology (RRCAT) in India. Microstructural analysis of the materials was carried out with the help of a JEOL-7610 field emission scanning electron microscope. A Thermofisher Scientific Nexsa base instrument, using an Al K α X-ray source, was employed to obtain the Mn 2p, Ni 2p, and Cu 2p X-ray photoelectron spectra (XPS) of the cathode samples.

2.3. Coin cell fabrication

CR2032 half cells were prepared using P3-NMNC as the working electrode. The electrolyte consisted of 1M NaClO₄ in a 1:1 volume ratio of ethylene carbonate (EC) and propylene carbonate (PC). The cathodes prepared contained the active material, PVDF binder, and Ketjen black in an 80:10:10 weight ratio. The active material loading of the cathode discs varied between 2 – 3 mg cm⁻².

2.4. Electrochemical studies

Keithley source meter unit (Model 2450-EC) was used to perform cyclic voltammetric tests (CV) at a scan rate of 0.1 mV s⁻¹. Other electrical experiments, such as Galvanostatic charge-discharge (GCD) testing and galvanostatic intermittent titration technique (GITT), were conducted using a Neware Battery Tester (Model no. CT-4008 T). Impedance measurements

on the P3-NMNC coin cells were conducted by applying an AC signal of 10 mV using an NF corp. LCR meter (model: ZM 2376) over a frequency range of 100 mHz to 1 MHz. *Operando* studies investigating phase transformations during electrochemical cycling were conducted using a synchrotron X-ray diffraction facility at Indus-2 (RRCAT). The X-ray diffraction utilized a beam with a wavelength of 0.6645 Å and an energy of 2.5 GeV.

3. RESULTS AND DISCUSSION

3.1. Structural characteristics

The composition of the P3 NaMn_{0.6}Ni_{0.3}Cu_{0.1}O₂ sample was confirmed using Inductively coupled plasma mass spectroscopy (ICP-MS), and the overall composition of the sample was Na_{0.988}Mn_{0.586}Ni_{0.305}Cu_{0.108}O₂. The crystal structure of the NaMn_{0.6}Ni_{0.3}Cu_{0.1}O₂ sample was analyzed using powder X-ray diffraction, and the corresponding room temperature (RT) XRD pattern is shown in Figure 1(a). The distinction between the O3 phase and P3 phase is primarily made by evaluating the ratio of the peak intensities between (104) and (015) peaks, given that both the phases have hexagonal symmetries, making peak positions indistinguishable (though the *c* parameters for O3 phase is lesser than that of P3). The P3 phase typically manifests a stronger (015) peak compared to the (104) peak in the XRD pattern, whereas the peak intensity ratio of the (015) to the (104) peaks is < 1 for the O3 phase.^{49, 50} As is evidenced by Figure 1(a), the I_{015} is significantly higher than I_{104} , suggesting that the NMNC sample is crystallized with a P3 structure.

Further, Rietveld refinement on the XRD data was carried out, and all the peaks were well fitted by the hexagonal P3 phase having the $R3m$ space group without any impurities. The calculated curve closely matches the experimental data with good reliability ($R_{wp} = 3.84$ and $\chi^2 = 1.39$). The crystallographic parameters *a* and *c* are 2.8865 ± 0.0003 Å and 16.7697 ± 0.0001 Å, respectively, with a unit cell volume of 121.003 ± 0.004 Å³. The detailed

refinement parameters are given in Table 1. Figure 1(a) inset provides a schematic illustration of the P3 crystal structure generated through VESTA.⁵¹

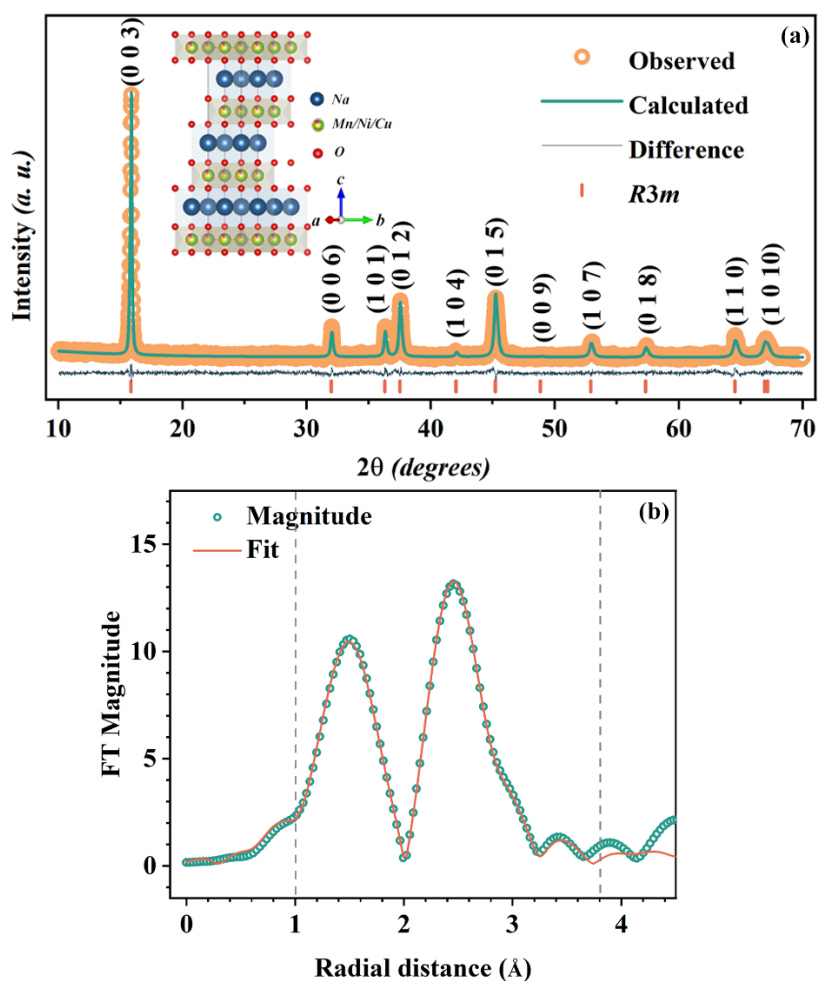


Figure 1. (a) Rietveld refinement profile of RT XRD data for P3-NMNC (inset shows the schematic of the P3 crystal structure). (b) Fourier transformation of the EXAFS spectrum along with the fitting profiles (fitting range of 1–3.8 Å) of P3-NMNC at the Mn K-edge.

Table 1. Crystallographic report of P3-NMNC obtained from the Rietveld refinement of RT XRD data.

| Atom | x | y | z | Occupancy | Site |
|------|---|---|------|-----------|------|
| Na | 0 | 0 | 0.17 | 1.00 | 3a |

| | | | | | |
|----------|---|---|------|----------------|----|
| Mn/Ni/Cu | 0 | 0 | 0 | 0.60/0.30/0.10 | 3a |
| O1 | 0 | 0 | 0.39 | 1.00 | 3a |
| O2 | 0 | 0 | 0.61 | 1.00 | 3a |

The extended X-ray absorption fine structure (EXAFS) data was analyzed at the Mn K-edge to investigate further the local environment around Mn-ions in the P3-NMNC material (Figure 1(b)). The Fourier transforms depict distinct peaks corresponding to TM-O and TM-TM coordination. The TM-O bond length obtained from the fitting aligns closely with that determined from the refinement of XRD data.

The microstructure of the P3-NMNC sample was probed using FESEM (Figure 2), and a predominance of spheroid particles of average size 291 ± 5 nm (standard deviation) is observed. A cathode material having smaller particles and less agglomeration facilitates a reduced Na-ion diffusion path compared to larger, densely agglomerated particles. Cathodes with small particles are expected to demonstrate higher specific capacities at elevated discharge rates, as Na-ions' movement in solid electrodes is the rate-limiting factor in Na-ion cells. While less noticeable at low discharge rates (~ 0.1 C), particle sizes become decisive in determining the achievable specific capacity at high C rates. The elemental mappings of P3-NMNC, depicted in Figure 2 (b1-b6), illustrate no segregation of constituent elements in the sample.

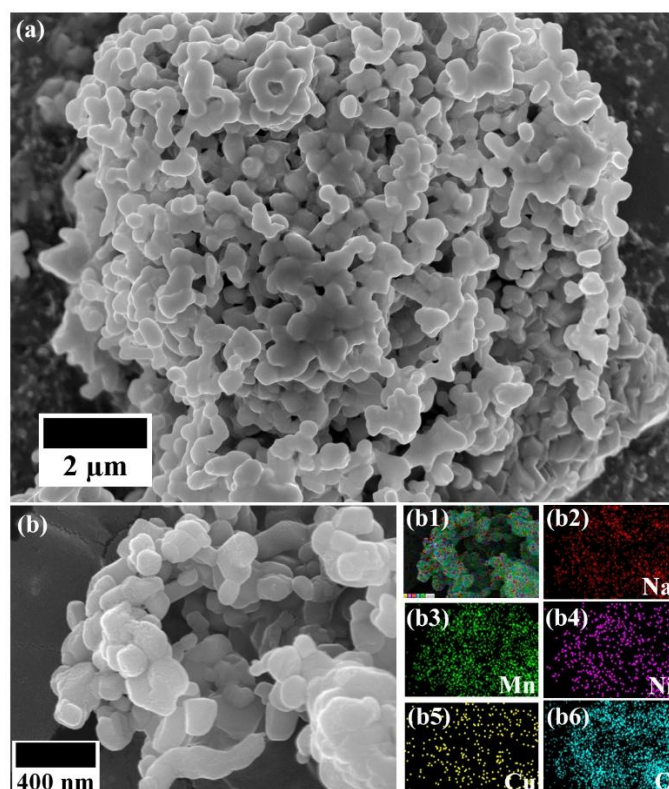


Figure 2. (a, b) SEM images of P3-NMNC. (b1-b6) Elemental mapping of P3-NMNC showing the distribution of constituent elements (Na, Mn, Ni, Cu, and O).

The oxidation states of Mn, Ni, and Cu in the P3-NMNC sample were confirmed using X-ray Photoelectron Spectroscopy (XPS), and Figure 3(a) displays the obtained spectra for Cu 2p, Mn 2p, and Ni 2p. The Mn 2p spectrum displays four peaks: ~ 641.8 eV and ~ 653.2 eV corresponding to Mn^{3+} and ~ 643.2 eV and ~ 654.7 eV associated with Mn^{4+} . This indicated that both Mn^{3+} and Mn^{4+} coexist in P3-NMNC.^{52, 53} In the Ni 2p spectrum, peaks corresponding to Ni 2p_{3/2} (~ 855 eV) and Ni 2p_{1/2} (~ 872 eV), along with their satellite peaks, confirm the presence of Ni in the 2+ oxidation state.^{52, 53} The peaks at ~ 933 eV and ~ 953 eV in the Cu 2p spectrum correspond to Cu 2p_{3/2} and Cu 2p_{1/2}, respectively, indicating that Cu also has a 2+ oxidation state in the material.^{52, 53}

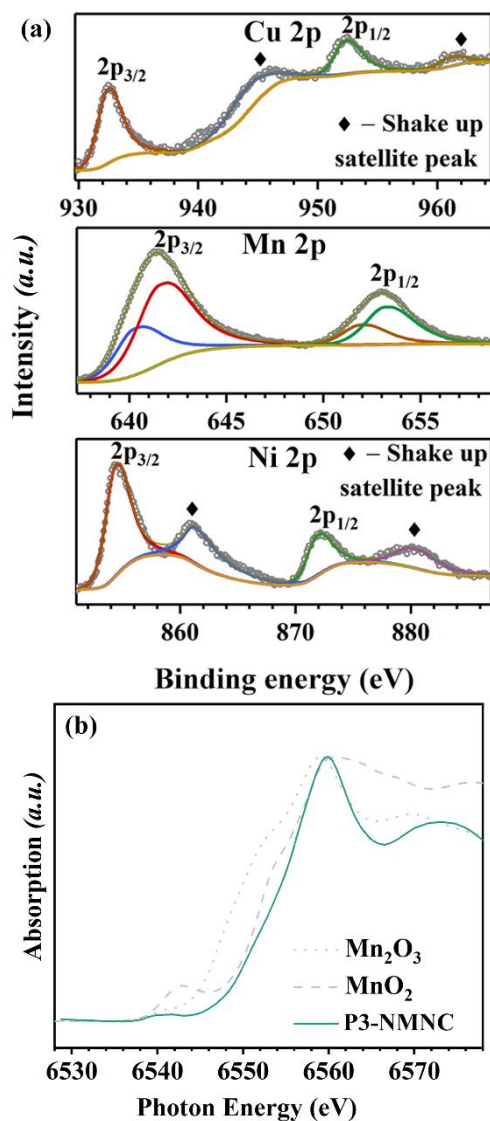


Figure 3. (a) XPS spectra of P3-NMNC sample. (b) XANES spectra at Mn K-edge of P3-NMNC.

The X-ray absorption near-edge structure (XANES) spectrum for P3-NMNC at the Mn K-edge is shown in Figure 3(b). The main peak in the Mn K-edge spectrum for NMNC lies between those for Mn_2O_3 and MnO_4 . This further confirms the co-existence of Mn^{3+} and Mn^{4+} in the sample.

3.2. Electrochemical Properties

The cyclic voltammetry (CV) analysis was done on the P3-NMNC cathode between 2.0 – 4.0 V and 2.0 – 4.2 V at a rate of 0.1 mV s^{-1} , and the CV curves are illustrated in Figure 4. Three distinct redox couples are identified at approximately 3.27/3.15 V, 3.35/3.23 V, and 3.69/3.53 V, as indicated by the labeled regions in Figure 4(a and b).^{44, 54, 55}

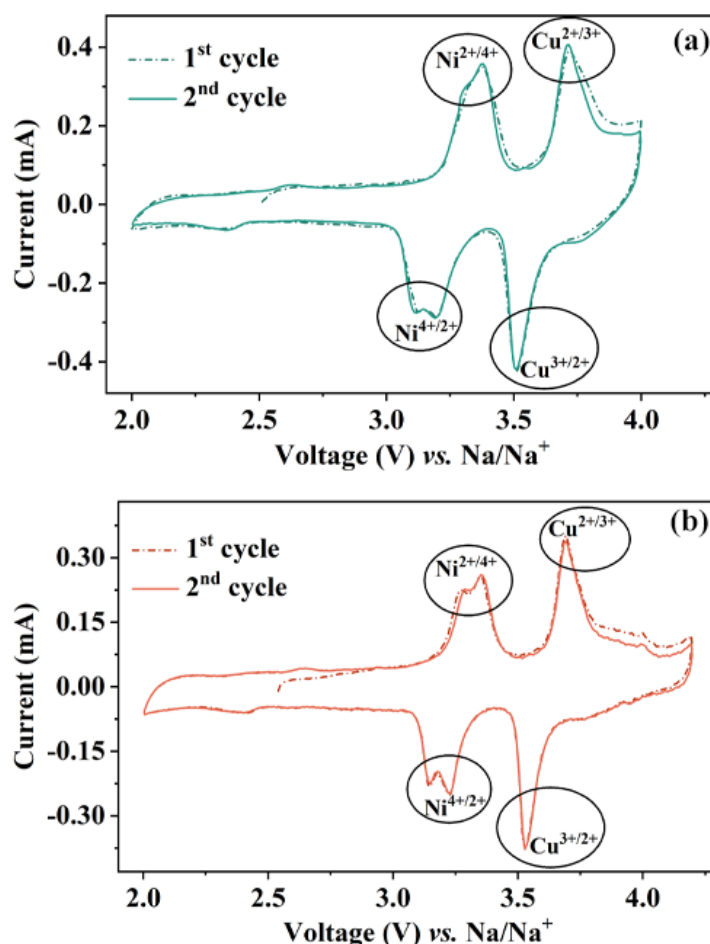


Figure 4. Cyclic voltammograms of P3-NMNC in the voltage range of (a) 2.0 – 4.0 V and (b) 2.0 – 4.2 V at a scan rate of 0.1 mV s^{-1} .

These peaks significantly contribute to the overall capacity of the electrode material. Further, the low-intensity redox peaks at around 2.60/2.38 V are associated with the $\text{Mn}^{3+}/\text{Mn}^{4+}$ redox reaction.^{56, 57} For the electrode cycled in a wider voltage window of 2.0 – 4.2 V, peaks observed above 4 V can be attributed to various phase transformations, as reported in literature.⁵⁶⁻⁵⁹

The electrochemical performance of P3-NMNC was investigated by conducting galvanostatic charge-discharge (GCD) tests at multiple current densities and in two voltage ranges of 2.0 – 4.0 V and 2.0 – 4.2 V. These two distinct upper cut-off voltages were chosen to examine the impact of phase transformations in the 4.0 – 4.2 V range on the electrochemical properties of P3-NMNC. The initial charge-discharge curve for P-NMNC at 0.1 C (Figure 5(a)) displays a plateau around 4.1 V during charging, while no such plateau is evident during discharging. Figure 5(b) presents the differential capacity versus voltage (dQ/dV vs. V) plot of first cycle for P3-NMNC cycled between 2.0 to 4.0 V. This plot reveals reversible peaks with oxidation/reduction occurring at 3.23/3.16 V, 3.31/3.25 V, and 3.64/3.56 V, aligning with results from CV analysis. On expanding the voltage range to 2.0 – 4.2 V, an additional oxidation peak at 4.1 V without a corresponding reduction peak appears in the dQ/dV vs. V plot (Figure 5(c)). Moreover, the intensity of this peak diminishes with cycling, as highlighted by the 2nd cycle differential capacity versus voltage (Figure 5(c) inset), contributing to the capacity fade observed with cyclability. As no transition metal in P3-NMNC exhibits redox activity at ~ 4.1 V, this feature likely arises from an unconventional anionic redox process and repeated phase transformations at elevated voltages.⁵⁸⁻⁶⁰ There are several studies probing the nature of anionic redox in layered oxides.⁶¹ Upon charging, oxygen evolution is attributed to the activity of peroxo-related⁶² and superoxo-related⁶³ species. The formation of superoxo-related species is particularly significant, as they are expected to react with propylene carbonate (PC) in the electrolyte, resulting in the formation of parasitic products arising from the breakdown of the solvent.⁶² An irreversible O₂ evolution observed during the initial charge is reported to be due to the instability of these superoxo-related species.⁶⁴

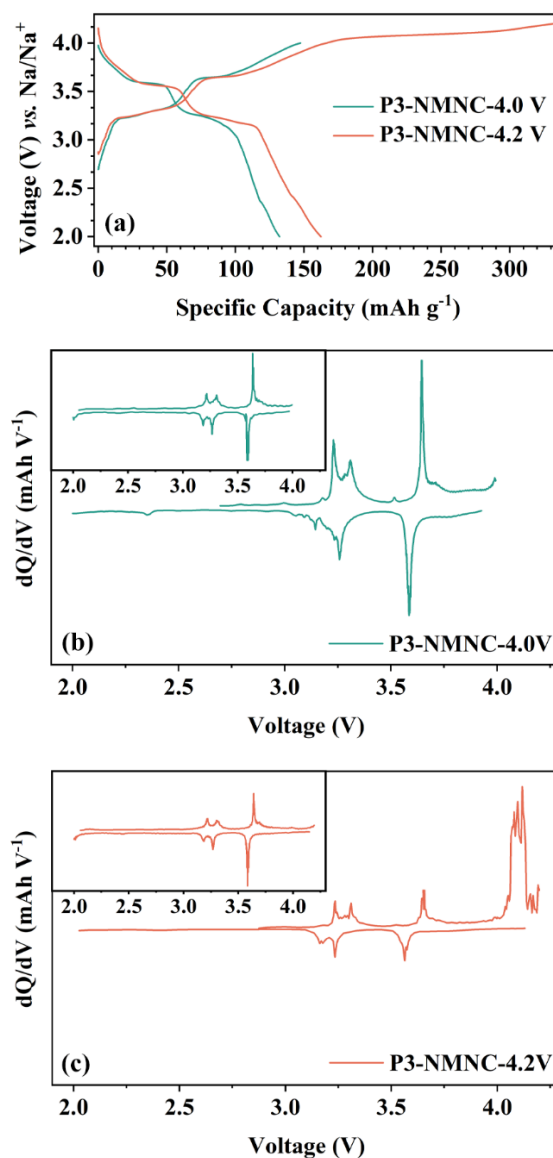


Figure 5. (a) The first charge-discharge cycle of P3-NMNC in the 2.0 – 4.0 V and 2.0 – 4.2 V ranges. First cycle dQ/dV vs. V plots of P3–NMNC in (b) 2.0 – 4.0 V and (c) 2.0 – 4.2 V range (insets show the dQ/dV vs. V plots of the second cycle).

Figure 6 shows the specific capacity & rate performance at various C rates and the cyclability of the P3-NMNC cathode in the two different voltage ranges. Figure 6(a) shows that at 0.1C, the P3-NMNC exhibits discharge specific capacities of 133 mAh g⁻¹, which declines to 124 mAh g⁻¹ (0.5C) and 120 mAh g⁻¹ (1C) when cycled in the voltage range of 2.0 – 4.0 V. Increasing the upper cut-off voltage to 4.2 V (Figure 6(b)), the specific capacity increases to

146 mAh g⁻¹, with values of 129 mAh g⁻¹ and 125 mAh g⁻¹ at a discharge rate of 0.5C and 1C, respectively. The voltage plateaus in the GCD profiles align with the peaks observed in the CV and dQ/dV vs. V curves. Table 2 compares the reported specific capacities of various layered oxide cathodes with P3-type structures at 0.1C.

Table 2. Comparison of discharge specific capacity of various layered oxides with P3-type structures.

| Material | Voltage Range (V) vs. Na ⁺ /Na | Specific Capacity at 0.1C (mAh g ⁻¹) | Rate performance (relative to 0.1C) | Capacity retention, cycles, C rate |
|---|---|--|-------------------------------------|------------------------------------|
| Na _{2/3} Ni _{1/3} Mn _{2/3} O ₂ ⁶⁵ | 2.5 – 4.15 | 86.2 | 52 % at 20C | 60%, 500 cycles, 1C |
| Na _{0.46} Ni _{0.21} Co _{0.11} Mn _{0.66} O ₂ ⁶⁶ | 2.1 – 4.3 | 135 | 54% at 5C | 58%, 200 cycles, 0.1C |
| Na _{0.6} Mn _{0.5} Co _{0.25} Ni _{0.25} O ₂ ⁶⁷ | 1.5 – 3.6 | 118 | – | 76%, 50 cycles, 0.1C |
| Na _{0.67} Mn _{0.67} Ni _{0.33} O ₂ ²⁹ | 2.0 – 4.1 | 90 | – | 70%, 350 cycles, 1C |
| Na _{2/3} Ni _{1/4} Mg _{1/12} Mn _{2/3} O ₂ ⁶⁸ | 2.0 – 4.4 | 125 | 48% at 20C | 66%, 100 cycles, 1C |
| Na _{0.67} Ni _{0.3} Cu _{0.03} Mn _{0.6} Ti _{0.07} O ₂ ⁶⁹ | 2.5 – 4.25 | 110 | 45% at 5C | 47%, 300 cycles, 1C |
| Na _{0.67} Ni _{0.24} Zn _{0.09} Mn _{0.67} O ₂ ⁷⁰ | 2.0 – 4.25 | 127 | 47% at 1000 mA g ⁻¹ | 62%, 50 cycles, 1C |
| Na _{0.67} Ni _{0.33} Mn _{0.637} Zr _{0.0335} O ₂ ⁷¹ | 2.0 – 4.0 | 90 | 87% at 100 mA g ⁻¹ | 83%, 100 cycles, 1C |
| NaMn _{0.6} Ni _{0.3} Cu _{0.1} O ₂ (<i>This work</i>) | 2.0 – 4.0 | 133 | 52% at 5C | 83%, 200 cycles, 1C |

| | | | | |
|--|-----------|-----|------------|---------------------|
| $\text{NaMn}_{0.6}\text{Ni}_{0.3}\text{Cu}_{0.1}\text{O}_2$ (<i>This work</i>) | 2.0 – 4.2 | 146 | 53 % at 5C | 74%, 100 cycles, 1C |
|--|-----------|-----|------------|---------------------|

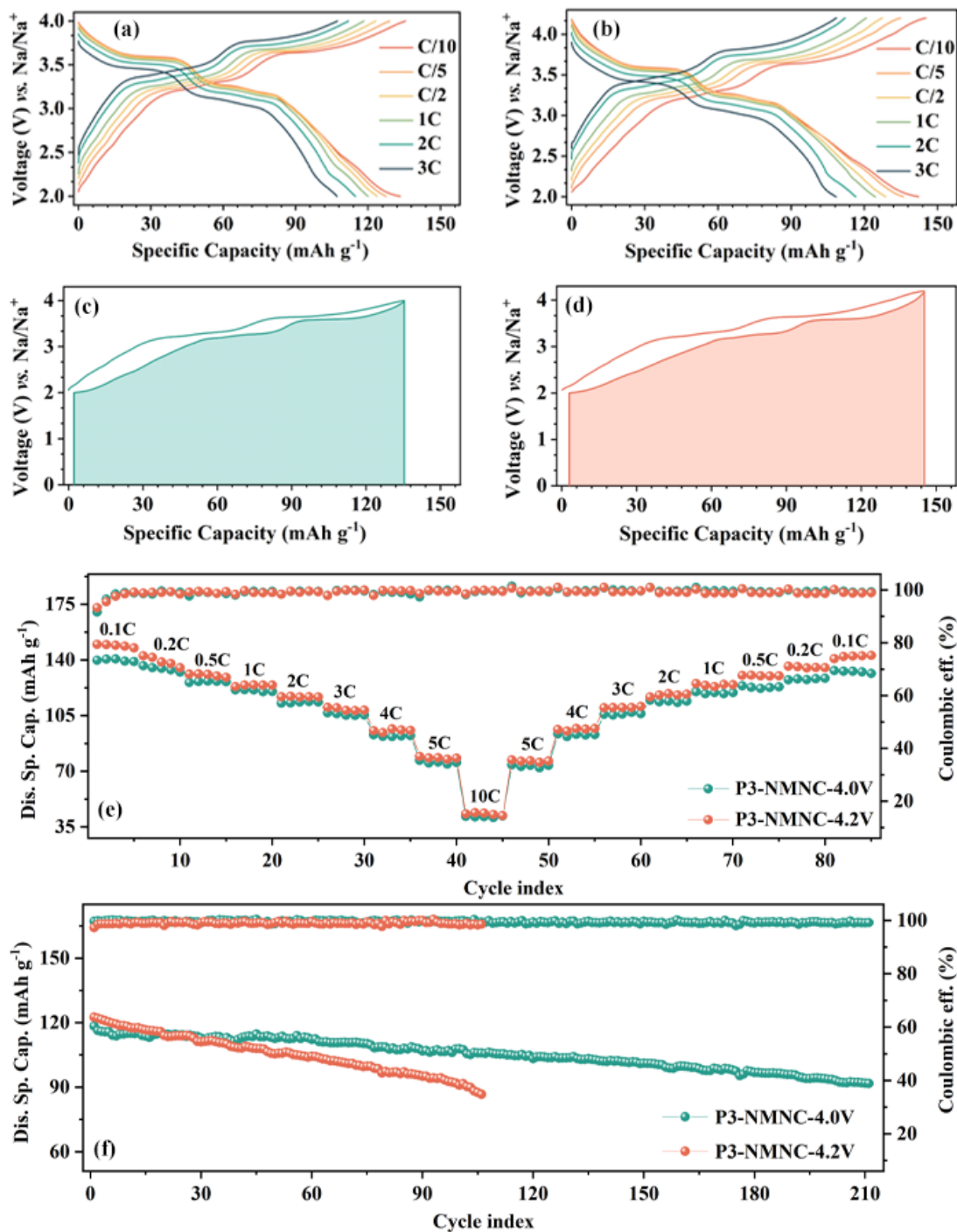


Figure 6. Galvanostatic charge-discharge curves of P3-NMNC in (a) 2.0 – 4.0 V and (b) 2.0 – 4.2 V range at selected C rates. The energy efficiency curves of P3-NMNC in (c) 2.0 – 4.0

V and (d) 2.0 – 4.2 V range at 0.1C. (e) Rate capability of the P3-NMNC sample. (f) Cyclic stability and coulombic efficiency of P3-NMNC at 1C.

Further, Figure 6(c and d) demonstrates the energy efficiency of the P3-NMNC cathode cycled in different voltage ranges (2.0 – 4.0 V and 2.0 – 4.2 V) at 0.1C. The region under the discharge curve (shaded part) represents the energy retrieved during discharge compared to the total energy input during charging (i.e., the area under the charging curve). The energy efficiency values for P3-NMNC cycled with upper cut-off voltages of 4.0V and 4.2V are 92% and 90%, respectively.

Figure 6(e) illustrates the rate capability of P3-NMNC samples charged to different voltages at various C rates from 0.1C to 10C. Increasing the discharge rate results in a decrease in discharge capacity across all samples. Nevertheless, when the discharge rate is reduced, all samples return to their initial discharge capacities, indicating reversible capacity loss with an increased C rate. Even at a discharge rate of 3C, the P3-NMNC demonstrates a discharge specific capacity of approximately 107 mAh g^{-1} , representing $\sim 87\%$ of the capacity observed at 1C. Increasing the C rate further to 10C leads to a significant decrease in the specific capacity ($\sim 45 \text{ mAh g}^{-1}$). As expected, the specific capacities are higher at all discharge rates when the cells are tested in the wider 2.0 – 4.2 V voltage range.

The cyclability of P3-NMNC samples was tested at 1C and 3C between 2.0 – 4.0 V & 2.0 – 4.2 V, and the results are shown in Figures 6(f) and S1. The P3-NMNC-4.0V and P3-NMNC-4.2V cathodes retained $\sim 80\%$ of the initial discharge capacity after 200 & 75 cycles, respectively, with a coulombic efficiency of $> 99\%$. Even at 3C, the cathodes retained $\sim 82\%$ (P3-NMNC-4.0V) and $\sim 50\%$ (P3-NMNC-4.2V) of their initial discharge capacities after 400 cycles (Figure S1). The cyclability data indicates that the cathode cycled up to 4.0 V retains higher capacity than P3-NMNC-4.2V. These results suggest that transformations occurring at

voltage values above 4.0 V degrade the cyclability. The influence of various transformations occurring beyond 4.0 V during charge-discharge on the cyclic stability is further discussed in the *operando* Synchrotron XRD section.

The Na⁺ diffusion dynamics in P3-NMNC cathodes upon desodiation/sodiation in different voltage ranges were probed by the galvanostatic intermittent titration technique (GITT), the results of which are illustrated in Figure 7. In this study, the cells underwent two cycles of charge and discharge prior to GITT measurements. A single unit in GITT involves the application of constant current for 10 minutes and a 30-minute relaxation period to attain a pseudo-equilibrium state. The Sodium-ion diffusion coefficient (D_{Na^+}) in the cathode materials is determined using Equation (1) ⁷²,

$$D_{Na^+} = \frac{4}{\pi\tau} \left(\frac{m_B V_m}{M_B S} \right)^2 \left(\frac{\Delta E_S}{\Delta E_\tau} \right)^2 \quad (t \ll L^2 / D) \quad (1)$$

where, τ represents the duration of the single constant current pulse, m_B corresponds to the active material mass loading, V_m & M_B denote the volume and mass of a single formula unit cell (FUC) of the cathode, and S is the surface area of the punched electrode. ΔE_S and ΔE_τ refer to equilibrium-state voltage and the change in the voltage during the constant current pulse, respectively. Figure 7(c) illustrates one GITT unit showing all these elements.

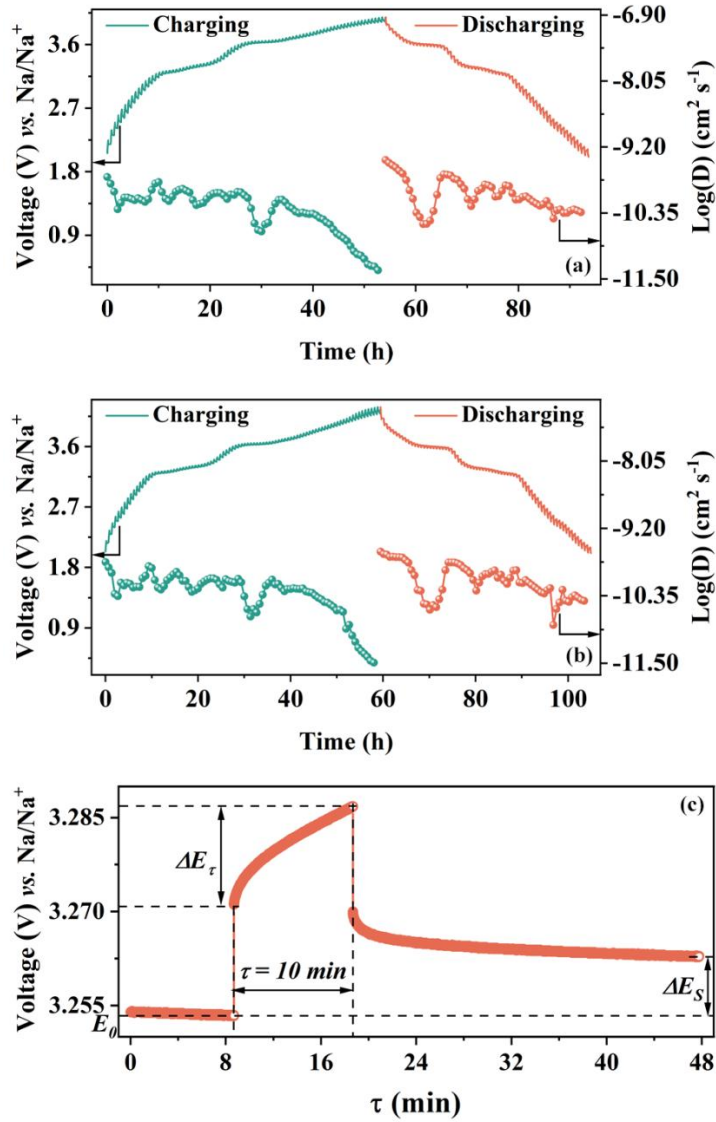


Figure 7. GITT profile of P3-NMNC in (a) 2.0 – 4.0 V and (b) 2.0 – 4.2 V range and the D_{Na^+} at different states of charge. (c) One titration unit in GITT.

From Figure 7(a and b), it is evident that the diffusion coefficient drops at elevated voltages during charging due to fewer Na⁺, suggesting a slower electrochemical process at these voltage levels. Similarly, as the cathode is fully laden with Na-ions during discharge, the diffusion coefficient decreases. D_{Na^+} values for P3-NMNC are between 6.15×10^{-12} to 3.38×10^{-10} cm² s⁻¹ and 3.46×10^{-12} to 2.18×10^{-10} cm² s⁻¹ for voltage cut-off of 4.0 V and 4.2 V,

respectively. The slightly lower diffusion coefficients observed in the sample cycled between 2.0 – 4.2 V could be due to the incidence of multiple phase transitions.

3.3. *Operando* SXRD

Analyses on the structural transformations occurring in P3-NMNC during cycling were conducted using *operando* Synchrotron XRD measurements. Figure 8(a) displays the XRD patterns during the first charge/discharge cycle at 0.1C, and the corresponding GCD curve is depicted in Figure 8(b). During the first desodiation process (up to ~ 3.61 V, Figure 8(a1)), the (003) and (006) peaks shift towards lower 2θ values caused by the movement of the transition metal layers to minimize the electrostatic repulsion. Nevertheless, all distinctive peaks of the P3 phase are observed without the emergence of any additional peaks. Additionally, the ratio of (104)/(015) is < 1 , indicating the absence of any P3 \rightarrow O3 phase transformation during this process. The (101) and (012) peaks of the P3 phase shift to higher values of 2θ , suggesting a reduction in the lattice parameter a of the P3 phase (Figure 8(a2)). Upon charging to ~ 4.05 V (Figure 8(b)), the P3 phase converts into a metastable P3' phase, which is highly reversible and causes only slight changes in lattice parameters, indicated by subtle shifts in peak positions.⁴² In the P3' phase, all Na-ions occupy one prismatic site, which is surrounded by TMO_6 octahedra sharing a face on one side and edges on the other⁷³. It is believed that the in-plane distortion in P3'-type compounds is less pronounced than that of distortions such as the O3' phase, making the P3' phase more stable than the monoclinic distortion of the O3 phase.²⁵

On charging the cell to voltages > 4.1 V, the intensity of the (104) peak increases, accompanied by a decrease in I_{015} . This shift causes the ratio of (104)/(015) to become > 1 , suggesting the appearance of an O3 phase (Figure 8(a3, a4)).^{32, 40, 74}

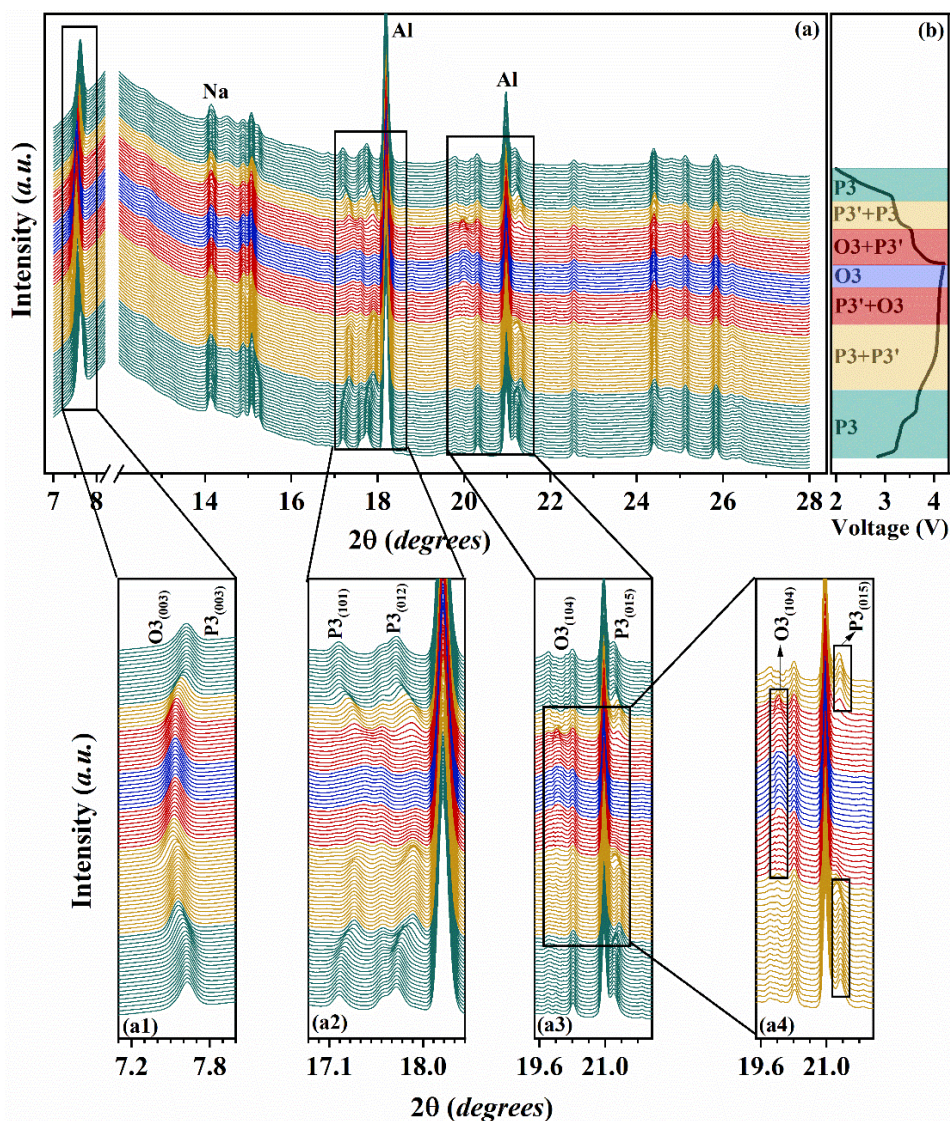


Figure 8. (a) *Operando* SXR D patterns of P3-NMNC sample at various states of charge (SOC) between 4.2 and 2.0 V during the first cycle charge/discharge cycle at 0.1C. Magnified view of (a1) (003) peak of P3, (a2) (101) & (012) peaks of P3, (a3, a4) (104) & (015) peaks of P3. (b) The corresponding GCD curve shows different SOC during *operando* measurements.

During discharge to 2.0 V, the O3 phase transforms to the initial P3 phase *via* the P3' at ~ 3.4 V. At the end of the first discharge, all the peaks revert to their primary positions without the emergence of any new diffraction peaks, signifying a reversible $P3 \leftrightarrow P3' \leftrightarrow O3$ transformation during charge/discharge.

While the emergence of an O3 phase above 4.1 V compels Na-ions to migrate through smaller tetrahedra, impacting rate performance, its direct influence on cyclability is limited. However, factors such as irreversible anionic redox activity at higher voltages leading to vacancy defects could significantly compromise the cyclability of the P3-NMNC cathode when cycled beyond 4.0 V. Additionally, changes in lattice parameters during repeated P3' \leftrightarrow O3 transformation generate strain; which damage the structural integrity of particles and the cathode membrane, further degrading the cyclic performance.

Electrochemical impedance spectroscopy (EIS) was done on fresh & cycled cells in the discharged state (discharged to 2.0 V) employing the P3-NMNC cathode materials. Figure S2 displays the RT Nyquist plots of the cells and the equivalent circuit (Figure S2a inset) for modeling the impedance data. In the equivalent circuit, R1 represents electrolyte resistance; (R2||CPE1) & (R3||CPE2) denote the contribution of electrodes-electrolyte interphase layer & charge transfer resistance, and CPE3 corresponds to the ion-diffusion in P3-NMNC. The overall cell resistances of both fresh cells are $\sim 95 \Omega$. A comparison of the cell resistances obtained from equivalent circuit fitting reveals an increase in overall cell resistance for both cells after cycling. The overall resistance of cycled P3-NMNC-4.0 V is $\sim 350 \Omega$, while that of P3-NMNC-4.2 V is $\sim 500 \Omega$, confirming that the increase in cell resistance is much higher when the cell is charged/discharged in the wider range of 2.0 – 4.2 V. These findings further confirm the subpar performance of the P3-NMNC cathode when cycled beyond 4.0 V.

4. CONCLUSIONS

In summary, a monophasic P3-type $\text{NaMn}_{0.6}\text{Ni}_{0.3}\text{Cu}_{0.1}\text{O}_2$ layered oxide is synthesized at 700 °C and evaluated for its structural characteristics. Further, the electrochemical performance of P3-NMNC as a potential positive electrode for Na^+ batteries is assessed in the 2.0 – 4.0 V and

2.0 – 4.2 V ranges. The P3-NMNC comprises spheroid-shaped particles that demonstrate exceptional rate capability, with specific capacity at 3C reaching 77% of that achieved at 0.1C. The structural changes in NMNC during charge-discharge cycles probed using *operando* SXRD reveal a reversible $P3 \leftrightarrow P3' \leftrightarrow O3$ transformation. Notably, the cell cycled in the narrower voltage range of 2.0 – 4.0 V exhibits a specific discharge capacity of ~ 133 mAh g⁻¹ at a current density equivalent to 0.1C. Moreover, it showcases excellent cyclability, retaining around 83% of its initial discharge capacity after 200 cycles at a discharge current corresponding to 1C. In contrast, cells cycled in the wider voltage range of 2.0 – 4.2 V experience rapid capacity degradation (falling below 80% of their initial capacity in just 75 cycles). This decline in performance is attributed to an irreversible anionic redox, substantiated by a distinctive peak observed in the dQ/dV vs. V plots in the 4.0 – 4.2 V range, and the repeated $P3' \leftrightarrow O3$ transformations resulting in strain due to changes in lattice parameters. These findings highlight the potential of low-temperature synthesized P3-type phases in advancing the development of layered oxide-based positive electrodes for Na⁺ batteries with better performance.

SUPPORTING INFORMATION

Cycle performance of P3-NMNC at 3C; Nyquist plots of the cells with P3-NMNC cathode.

AUTHOR INFORMATION

Corresponding Author

Sunil Kumar – Department of Metallurgical Engineering and Materials Science, Indian Institute of Technology Indore, Simrol, 453552, India; E-mail: sunil@iiti.ac.in

Authors

Samridhhi Saxena – Department of Metallurgical Engineering and Materials Science, Indian Institute of Technology Indore, Simrol, 453552, India

Manish Badole – Department of Metallurgical Engineering and Materials Science, Indian Institute of Technology Indore, Simrol, 453552, India

Hari Narayanan Vasavan – Department of Metallurgical Engineering and Materials Science, Indian Institute of Technology Indore, Simrol, 453552, India

Velaga Srihari – High Pressure & Synchrotron Radiation Physics Division, Bhabha Atomic Research Centre, Mumbai, 400085, India

Asish Kumar Das – Department of Metallurgical Engineering and Materials Science, Indian Institute of Technology Indore, Simrol, 453552, India

Pratiksha Gami – Department of Metallurgical Engineering and Materials Science, Indian Institute of Technology Indore, Simrol, 453552, India

Neha Dagar – Department of Metallurgical Engineering and Materials Science, Indian Institute of Technology Indore, Simrol, 453552, India

Sonia Deswal – School of Physical Sciences, Indian Institute of Technology Mandi, Mandi, 175005, India

Pradeep Kumar – School of Physical Sciences, Indian Institute of Technology Mandi, Mandi, 175005, India

Himanshu Kumar Poswal – High Pressure & Synchrotron Radiation Physics Division, Bhabha Atomic Research Centre, Mumbai, 400085, India

Author Contributions

The manuscript was written with contributions from all authors. All authors have approved the final version of the manuscript.

Notes

The authors declare no competing financial interest.

ACKNOWLEDGMENTS

This work was financially supported by the Science and Engineering Research Board, Govt. of India (grant number: CRG/2021/005548) and the Prime Minister's Research Fellowship, Ministry of Education, Government of India (grant number: 2103359). The authors acknowledge Dr. Biplab Ghosh for his help in recording the XAS spectra at RRCAT, Indore, India.

References

- (1) Tarascon, J. M.; Armand, M. Issues and challenges facing rechargeable lithium batteries. *Nature* **2001**, *414* (6861), 359-367. <https://doi.org/10.1038/35104644>.
- (2) Goodenough, J. B.; Kim, Y. Challenges for Rechargeable Li Batteries. *Chem. Mater.* **2010**, *22* (3), 587-603. <https://doi.org/10.1021/cm901452z>.
- (3) Hu, Y.-S.; Komaba, S.; Forsyth, M.; Johnson, C.; Rojo, T. A New Emerging Technology: Na-Ion Batteries. *Small Methods* **2019**, *3* (4), 1900184. <https://doi.org/10.1002/smt.201900184>.
- (4) Hwang, J.-Y.; Myung, S.-T.; Sun, Y.-K. Sodium-ion batteries: present and future. *Chem. Soc. Rev.* **2017**, *46* (12), 3529-3614, 10.1039/C6CS00776G. <https://doi.org/10.1039/C6CS00776G>.
- (5) Yabuuchi, N.; Kubota, K.; Dahbi, M.; Komaba, S. Research Development on Sodium-Ion Batteries. *Chem. Rev.* **2014**, *114* (23), 11636-11682. <https://doi.org/10.1021/cr500192f>.

- (6) Nayak, P. K.; Yang, L.; Brehm, W.; Adelhelm, P. From Lithium-Ion to Sodium-Ion Batteries: Advantages, Challenges, and Surprises. *Angew. Chem. Int. Ed.* **2018**, *57* (1), 102-120. <https://doi.org/10.1002/anie.201703772>.
- (7) Kim, S.-W.; Seo, D.-H.; Ma, X.; Ceder, G.; Kang, K. Electrode Materials for Rechargeable Sodium-Ion Batteries: Potential Alternatives to Current Lithium-Ion Batteries. *Adv. Energy Mater.* **2012**, *2* (7), 710-721. <https://doi.org/10.1002/aenm.201200026>.
- (8) Palomares, V.; Serras, P.; Villaluenga, I.; Hueso, K. B.; Carretero-González, J.; Rojo, T. Na-ion batteries, recent advances and present challenges to become low cost energy storage systems. *Energy Environ. Sci.* **2012**, *5* (3), 5884-5901, 10.1039/C2EE02781J. <https://doi.org/10.1039/C2EE02781J>.
- (9) Chen, M.; Liu, Q.; Wang, S.-W.; Wang, E.; Guo, X.; Chou, S.-L. High-Abundance and Low-Cost Metal-Based Cathode Materials for Sodium-Ion Batteries: Problems, Progress, and Key Technologies. *Adv. Energy Mater.* **2019**, *9* (14), 1803609. <https://doi.org/10.1002/aenm.201803609>.
- (10) Vasavan, H. N.; Badole, M.; Saxena, S.; Das, A. K.; Deswal, S.; Kumar, P.; Kumar, S. Excellent Structural Stability-Driven Cyclability in P2-Type Ti-Based Cathode for Na-Ion Batteries. *ACS Appl. Energy Mater.* **2023**, *6* (4), 2440-2447. <https://doi.org/10.1021/acsaem.2c03750>.
- (11) Zhang, Z.; Du, Y.; Wang, Q.-C.; Xu, J.; Zhou, Y.-N.; Bao, J.; Shen, J.; Zhou, X. A Yolk-Shell-Structured FePO₄ Cathode for High-Rate and Long-Cycling Sodium-Ion Batteries. *Angew. Chem. Int. Ed.* **2020**, *59* (40), 17504-17510. <https://doi.org/10.1002/anie.202008318>.

- (12) Qing Xue, S. L., Yanan Zhao, Peng Sheng, Li Xu, Zhengxi Li, Bo Zhang, Hui Li, Bo Wang, Libin Yang, Yuliang Cao, Zhongxue Chen. Novel Alkaline Sodium-Ion Battery Capacitor Based on Active Carbon||Na_{0.44}MnO₂ towards Low Cost, High-Rate Capability and Long-Term Lifespan. *Acta Phys. -Chim. Sin.* **2024**, *40* (2), 2303041-. <https://doi.org/10.3866/pku.Whxb202303041>.
- (13) Liu, Q.; Hu, Z.; Chen, M.; Zou, C.; Jin, H.; Wang, S.; Chou, S.-L.; Dou, S.-X. Recent Progress of Layered Transition Metal Oxide Cathodes for Sodium-Ion Batteries. *Small* **2019**, *15* (32), 1805381. <https://doi.org/10.1002/sml.201805381>.
- (14) Darga, J.; Lamb, J.; Manthiram, A. Industrialization of Layered Oxide Cathodes for Lithium-Ion and Sodium-Ion Batteries: A Comparative Perspective. *Energy Technol.* **2020**, *8* (12), 2000723. <https://doi.org/10.1002/ente.202000723>.
- (15) Delmas, C.; Carlier, D.; Guignard, M. The Layered Oxides in Lithium and Sodium-Ion Batteries: A Solid-State Chemistry Approach. *Adv. Energy Mater.* **2021**, *11* (2), 2001201. <https://doi.org/10.1002/aenm.202001201>.
- (16) Vasavan, H. N.; Badole, M.; Dwivedi, S.; Kumar, D.; Kumar, P.; Kumar, S. Enhanced rate performance and specific capacity in Ti-substituted P2-type layered oxide enabled by crystal structure and particle morphology modifications. *Chem. Eng. J.* **2022**, *448*, 137662. <https://doi.org/10.1016/j.cej.2022.137662>.
- (17) Tang, H.; Duan, L.; Liao, J.; Sheng, X.; Xu, J.; Zhou, X. Magnesium ion-doped layered oxide cathodes for alkali-metal ion batteries: Recent research progress and outlook. *Energy Storage Mater.* **2023**, *62*, 102935. <https://doi.org/10.1016/j.ensm.2023.102935>.

- (18) Delmas, C.; Fouassier, C.; Hagenmuller, P. Structural classification and properties of the layered oxides. *Physica B+C* **1980**, *99* (1), 81-85. [https://doi.org/10.1016/0378-4363\(80\)90214-4](https://doi.org/10.1016/0378-4363(80)90214-4).
- (19) Kubota, K.; Kumakura, S.; Yoda, Y.; Kuroki, K.; Komaba, S. Electrochemistry and Solid-State Chemistry of NaMeO₂ (Me = 3d Transition Metals). *Adv. Energy Mater.* **2018**, *8* (17), 1703415. <https://doi.org/10.1002/aenm.201703415>.
- (20) Liu, Y.; Fang, X.; Zhang, A.; Shen, C.; Liu, Q.; Enaya, H. A.; Zhou, C. Layered P2-Na_{2/3}[Ni_{1/3}Mn_{2/3}]O₂ as high-voltage cathode for sodium-ion batteries: The capacity decay mechanism and Al₂O₃ surface modification. *Nano energy* **2016**, *27*, 27-34. <https://doi.org/10.1016/j.nanoen.2016.06.026>.
- (21) Lu, Z.; Dahn, J. R. In Situ X-Ray Diffraction Study of P2 - Na_{2/3} [Ni_{1/3}Mn_{2/3}] O₂. *J. Electrochem. Soc.* **2001**, *148* (11), A1225. <https://doi.org/10.1149/1.1407247>.
- (22) Wang, H.; Yang, B.; Liao, X.-Z.; Xu, J.; Yang, D.; He, Y.-S.; Ma, Z.-F. Electrochemical properties of P2-Na_{2/3}[Ni_{1/3}Mn_{2/3}]O₂ cathode material for sodium ion batteries when cycled in different voltage ranges. *Electrochim. Acta* **2013**, *113*, 200-204. <https://doi.org/10.1016/j.electacta.2013.09.098>.
- (23) Wang, P.-F.; You, Y.; Yin, Y.-X.; Wang, Y.-S.; Wan, L.-J.; Gu, L.; Guo, Y.-G. Suppressing the P2–O2 Phase Transition of Na_{0.67}Mn_{0.67}Ni_{0.33}O₂ by Magnesium Substitution for Improved Sodium-Ion Batteries. *Angew. Chem. Int. Ed.* **2016**, *55* (26), 7445-7449. <https://doi.org/10.1002/anie.201602202>.
- (24) Wang, P.-F.; You, Y.; Yin, Y.-X.; Guo, Y.-G. An O3-type NaNi_{0.5}Mn_{0.5}O₂ cathode for sodium-ion batteries with improved rate performance and cycling stability. *J. Mater. Chem. A* **2016**, *4* (45), 17660-17664, 10.1039/C6TA07589D. <https://doi.org/10.1039/C6TA07589D>.

- (25) Komaba, S.; Yabuuchi, N.; Nakayama, T.; Ogata, A.; Ishikawa, T.; Nakai, I. Study on the Reversible Electrode Reaction of $\text{Na}_{1-x}\text{Ni}_{0.5}\text{Mn}_{0.5}\text{O}_2$ for a Rechargeable Sodium-Ion Battery. *Inorg. Chem.* **2012**, *51* (11), 6211-6220. <https://doi.org/10.1021/ic300357d>.
- (26) Komaba, S.; Nakayama, T.; Ogata, A.; Shimizu, T.; Takei, C.; Takada, S.; Hokura, A.; Nakai, I. Electrochemically Reversible Sodium Intercalation of Layered $\text{NaNi}_{0.5}\text{Mn}_{0.5}\text{O}_2$ and NaCrO_2 . *ECS Transactions* **2009**, *16* (42), 43. <https://doi.org/10.1149/1.3112727>.
- (27) Vasavan, H. N.; Badole, M.; Dwivedi, S.; Kumar, S. Structural and transport properties of P2-Type $\text{Na}_{0.70}\text{Ni}_{0.20}\text{Cu}_{0.15}\text{Mn}_{0.65}\text{O}_2$ layered oxide. *Ceram. Int.* **2022**, *48* (19, Part B), 28986-28993. <https://doi.org/10.1016/j.ceramint.2022.04.206>.
- (28) Zhang, L.; Wang, J.; Li, J.; Schuck, G.; Winter, M.; Schumacher, G.; Li, J. Preferential occupation of Na in P3-type layered cathode material for sodium ion batteries. *Nano energy* **2020**, *70*, 104535. <https://doi.org/10.1016/j.nanoen.2020.104535>.
- (29) Zhang, L.; Wang, J.; Schuck, G.; Xi, F.; Du, L.; Winter, M.; Schumacher, G.; Li, J. Stabilizing P3-Type Oxides as Cathodes for High-Rate and Long-Life Sodium Ion Batteries by Disordered Distribution of Transition Metals. *Small Methods* **2020**, *4* (10), 2000422. <https://doi.org/10.1002/smt.202000422>.
- (30) Chen, G.; Ji, H.; Fang, H.; Zhai, J.; Ma, Z.; Ji, W.; Wang, Y.; Huang, Y.; Liu, L.; Tong, W.; et al. Dual Modification of P3-Type Layered Cathodes to Achieve High Capacity and Long Cyclability for Sodium-Ion Batteries. *ACS Appl. Mater. Interfaces* **2023**, *15* (28), 33682-33692. <https://doi.org/10.1021/acsami.3c06375>.
- (31) Guo, S.; Sun, Y.; Yi, J.; Zhu, K.; Liu, P.; Zhu, Y.; Zhu, G.-z.; Chen, M.; Ishida, M.; Zhou, H. Understanding sodium-ion diffusion in layered P2 and P3 oxides via experiments

and first-principles calculations: a bridge between crystal structure and electrochemical performance. *NPG Asia Mater.* **2016**, *8* (4), e266-e266. <https://doi.org/10.1038/am.2016.53>.

(32) Song, B.; Hu, E.; Liu, J.; Zhang, Y.; Yang, X.-Q.; Nanda, J.; Huq, A.; Page, K. A novel P3-type $\text{Na}_{2/3}\text{Mg}_{1/3}\text{Mn}_{2/3}\text{O}_2$ as high capacity sodium-ion cathode using reversible oxygen redox. *J. Mater. Chem. A* **2019**, *7* (4), 1491-1498, 10.1039/C8TA09422E. <https://doi.org/10.1039/C8TA09422E>.

(33) Hou, P.; Dong, M.; Lin, Z.; Sun, Z.; Gong, M.; Li, F.; Xu, X. Alleviating the Jahn–Teller Distortion of P3-Type Manganese-Based Cathodes by Compositionally Graded Structure for Sodium-Ion Batteries. *ACS Sustain. Chem. Eng* **2023**, *11* (29), 10785-10794. <https://doi.org/10.1021/acssuschemeng.3c01854>.

(34) Li, Q.; Qiao, Y.; Guo, S.; Jiang, K.; Li, Q.; Wu, J.; Zhou, H. Both Cationic and Anionic Co-(de)intercalation into a Metal-Oxide Material. *Joule* **2018**, *2* (6), 1134-1145. <https://doi.org/10.1016/j.joule.2018.03.010>.

(35) Vasavan, H. N.; Badole, M.; Saxena, S.; Srihari, V.; Das, A. K.; Gami, P.; Deswal, S.; Kumar, P.; Kumar, S. Unveiling the Potential of P3 Phase in Enhancing the Electrochemical Performance of a Layered Oxide Cathode. *Mater. Today Energy* **2023**, 101380. <https://doi.org/10.1016/j.mtener.2023.101380>.

(36) Vasavan, H. N.; Badole, M.; Saxena, S.; Srihari, V.; Das, A. K.; Gami, P.; Deswal, S.; Kumar, P.; Kumar, S. Impact of P3/P2 mixed phase on the structural and electrochemical performance of $\text{Na}_{0.75}\text{Mn}_{0.75}\text{Al}_{0.25}\text{O}_2$ cathode. *J. Energy Storage* **2023**, *74*, 109428. <https://doi.org/10.1016/j.est.2023.109428>.

(37) Ramesh, A.; Tripathi, A.; Bosman, M.; Xi, S.; Balaya, P. Enhancement in rate performance and high voltage structural stability of P3/O3 $\text{Na}_{0.9}\text{Fe}_{0.5}\text{Mn}_{0.45}\text{Ni}_{0.05}\text{O}_2$ layered

oxide cathode. *J. Electroanal. Chem.* **2023**, 932, 117222.

<https://doi.org/10.1016/j.jelechem.2023.117222>.

(38) Li, R.; Gao, J.; Li, J.; Huang, H.; Li, X.; Wang, W.; Zheng, L.-R.; Hao, S.-M.; Qiu, J.; Zhou, W. An Undoped Tri-Phase Coexistent Cathode Material for Sodium-Ion Batteries. *Adv. Funct. Mater.* **2022**, 32 (41), 2205661. <https://doi.org/10.1002/adfm.202205661>.

(39) Huang, Q.; Xu, S.; Xiao, L.; He, P.; Liu, J.; Yang, Y.; Wang, P.; Huang, B.; Wei, W. Improving the Electrochemical Properties of the Manganese-Based P3 Phase by Multiphasic Intergrowth. *Inorg. Chem.* **2018**, 57 (24), 15584-15591. <https://doi.org/10.1021/acs.inorgchem.8b02931>.

(40) Risthaus, T.; Chen, L.; Wang, J.; Li, J.; Zhou, D.; Zhang, L.; Ning, D.; Cao, X.; Zhang, X.; Schumacher, G.; et al. P3 Na_{0.9}Ni_{0.5}Mn_{0.5}O₂ Cathode Material for Sodium Ion Batteries. *Chem. Mater.* **2019**, 31 (15), 5376-5383. <https://doi.org/10.1021/acs.chemmater.8b03270>.

(41) Tripathi, A.; Xi, S.; Gajjela, S. R.; Balaya, P. Introducing Na-sufficient P3-Na_{0.9}Fe_{0.5}Mn_{0.5}O₂ as a cathode material for Na-ion batteries. *Chem. Commun.* **2020**, 56 (73), 10686-10689, 10.1039/D0CC03701J. <https://doi.org/10.1039/D0CC03701J>.

(42) Shi, Y.; Zhang, Z.; Jiang, P.; Gao, A.; Li, K.; Zhang, Q.; Sun, Y.; Lu, X.; Cao, D.; Lu, X. Unlocking the potential of P3 structure for practical Sodium-ion batteries by fabricating zero strain framework for Na⁺ intercalation. *Energy Storage Mater.* **2021**, 37, 354-362. <https://doi.org/10.1016/j.ensm.2021.02.020>.

(43) Yang, L.; Sun, Y.; Adelhelm, P. Electrochemical Properties of Layered Na_xNi_{x/2}Mn_{1-x/2}O₂ (0.5 ≤ x ≤ 1.1) with P3 Structure as Cathode for Sodium-Ion Batteries. *Energy Technol.* **2022**, 10 (4), 2101121. <http://dx.doi.org/10.18452/26150>.

- (44) Ma, P.; Kang, W.; Wang, Y.; Cao, D.; Fan, L.; Sun, D. Binary metal co-substituted P2-type $\text{Na}_{0.67}\text{Mn}_{0.7}\text{Cu}_{0.15}\text{Ni}_{0.15}\text{O}_2$ microspheres as robust cathode for high-power sodium ion battery. *Appl. Surf. Sci.* **2020**, *529*, 147105. <https://doi.org/10.1016/j.apsusc.2020.147105>.
- (45) Yang, L.; Luo, S.-h.; Wang, Y.; Zhan, Y.; Wang, Q.; Zhang, Y.; Liu, X.; Mu, W.; Teng, F. Cu-doped layered P2-type $\text{Na}_{0.67}\text{Ni}_{0.33-x}\text{Cu}_x\text{Mn}_{0.67}\text{O}_2$ cathode electrode material with enhanced electrochemical performance for sodium-ion batteries. *Chem. Eng. J.* **2021**, *404*, 126578. <https://doi.org/10.1016/j.cej.2020.126578>.
- (46) Saxena, S.; Vasavan, H. N.; Badole, M.; Das, A. K.; Deswal, S.; Kumar, P.; Kumar, S. Tailored P2/O3 phase-dependent electrochemical behavior of Mn-based cathode for sodium-ion batteries. *J. Energy Storage* **2023**, *64*, 107242. <https://doi.org/10.1016/j.est.2023.107242>.
- (47) Saxena, S.; Badole, M.; Vasavan, H. N.; Srihari, V.; Das, A. K.; Gami, P.; Deswal, S.; Kumar, P.; Kumar, S. Deciphering the role of optimal P2/O3 phase fraction in enhanced cyclability and specific capacity of layered oxide cathodes. *Chem. Eng. J.* **2024**, *485*, 149921. <https://doi.org/10.1016/j.cej.2024.149921>.
- (48) Coelho, A. TOPAS and TOPAS-Academic: an optimization program integrating computer algebra and crystallographic objects written in C++. *J. Appl. Crystallogr.* **2018**, *51* (1), 210-218. <https://doi.org/10.1107/S1600576718000183>.
- (49) Bo, S.-H.; Li, X.; Toumar, A. J.; Ceder, G. Layered-to-Rock-Salt Transformation in Desodiated Na_xCrO_2 ($x = 0.4$). *Chem. Mater.* **2016**, *28* (5), 1419-1429. <https://doi.org/10.1021/acs.chemmater.5b04626>.
- (50) Lei, Y.; Li, X.; Liu, L.; Ceder, G. Synthesis and Stoichiometry of Different Layered Sodium Cobalt Oxides. *Chem. Mater.* **2014**, *26* (18), 5288-5296. <https://doi.org/10.1021/cm5021788>.

- (51) Momma, K.; Izumi, F. VESTA 3 for three-dimensional visualization of crystal, volumetric and morphology data. *J. Appl. Crystallogr.* **2011**, *44* (6), 1272-1276. <https://doi.org/10.1107/S0021889811038970>.
- (52) Chastain, J.; King Jr, R. C. Handbook of X-ray photoelectron spectroscopy. *Perkin-Elmer Corporation* **1992**, *40*, 221.
- (53) Hüfner, S. *Photoelectron spectroscopy: principles and applications*; Springer Science & Business Media, 2013.
- (54) Wang, L.; Sun, Y.-G.; Hu, L.-L.; Piao, J.-Y.; Guo, J.; Manthiram, A.; Ma, J.; Cao, A.-M. Copper-substituted $\text{Na}_{0.67}\text{Ni}_{0.3-x}\text{Cu}_x\text{Mn}_{0.7}\text{O}_2$ cathode materials for sodium-ion batteries with suppressed P2–O2 phase transition. *J. Mater. Chem. A* **2017**, *5* (18), 8752-8761, 10.1039/C7TA00880E. <https://doi.org/10.1039/C7TA00880E>.
- (55) Paidi, A. K.; Park, W. B.; Ramakrishnan, P.; Lee, S.-H.; Lee, J.-W.; Lee, K.-S.; Ahn, H.; Liu, T.; Gim, J.; Avdeev, M.; et al. Unravelling the Nature of the Intrinsic Complex Structure of Binary-Phase Na-Layered Oxides. *Adv. Mater.* **2022**, *34* (29), 2202137. <https://doi.org/10.1002/adma.202202137>.
- (56) Cheng, J.-H.; Pan, C.-J.; Lee, J.-F.; Chen, J.-M.; Guignard, M.; Delmas, C.; Carlier, D.; Hwang, B.-J. Simultaneous Reduction of Co^{3+} and Mn^{4+} in P2- $\text{Na}_{2/3}\text{Co}_{2/3}\text{Mn}_{1/3}\text{O}_2$ As Evidenced by X-ray Absorption Spectroscopy during Electrochemical Sodium Intercalation. *Chem. Mater.* **2014**, *26* (2), 1219-1225. <https://doi.org/10.1021/cm403597h>.
- (57) Kang, S. M.; Kim, D.; Lee, K.-S.; Kim, M.-S.; Jin, A.; Park, J.-H.; Ahn, C.-Y.; Jeon, T.-Y.; Jung, Y. H.; Yu, S.-H.; et al. Structural and Thermodynamic Understandings in Mn-Based Sodium Layered Oxides during Anionic Redox. *Adv. Sci.* **2020**, *7* (16), 2001263. <https://doi.org/10.1002/advs.202001263>.

(58) Rong, X.; Liu, J.; Hu, E.; Liu, Y.; Wang, Y.; Wu, J.; Yu, X.; Page, K.; Hu, Y.-S.; Yang, W.; et al. Structure-Induced Reversible Anionic Redox Activity in Na Layered Oxide Cathode. *Joule* **2018**, *2* (1), 125-140. <https://doi.org/10.1016/j.joule.2017.10.008>.

(59) Zheng, W.; Liang, G.; Zhang, S.; Davey, K.; Guo, Z. Understanding voltage hysteresis and decay during anionic redox reaction in layered transition metal oxide cathodes: A critical review. *Nano Res.* **2023**, *16* (3), 3766-3780. <https://doi.org/10.1007/s12274-022-5003-1>.

(60) Kim, E. J.; Mofredj, K.; Pickup, D. M.; Chadwick, A. V.; Irvine, J. T. S.; Armstrong, A. R. Activation of anion redox in P3 structure cobalt-doped sodium manganese oxide via introduction of transition metal vacancies. *J. Power Sources* **2021**, *481*, 229010. <https://doi.org/10.1016/j.jpowsour.2020.229010>.

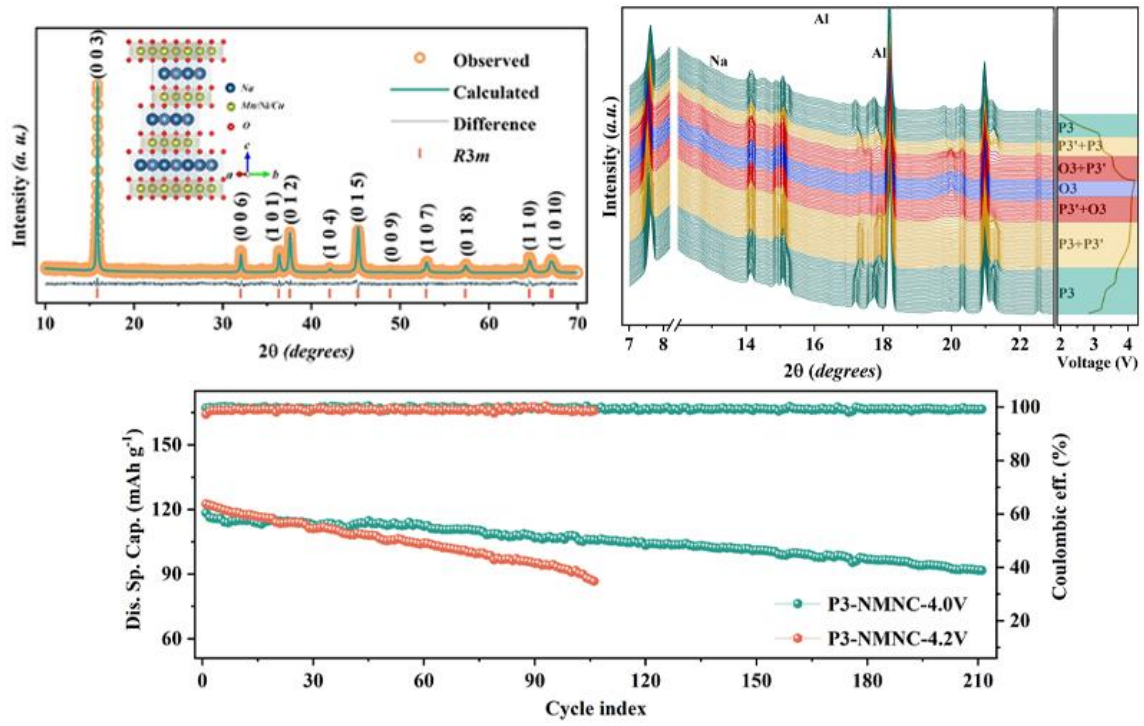
(61) Ren, H.; Li, Y.; Ni, Q.; Bai, Y.; Zhao, H.; Wu, C. Unraveling Anionic Redox for Sodium Layered Oxide Cathodes: Breakthroughs and Perspectives. *Adv. Mater.* **2022**, *34* (8), 2106171. <https://doi.org/10.1002/adma.202106171>.

(62) Qiao, Y.; Guo, S.; Zhu, K.; Liu, P.; Li, X.; Jiang, K.; Sun, C.-J.; Chen, M.; Zhou, H. Reversible anionic redox activity in Na₃RuO₄ cathodes: a prototype Na-rich layered oxide. *Energy Environ. Sci.* **2018**, *11* (2), 299-305, 10.1039/C7EE03554C. <https://doi.org/10.1039/C7EE03554C>.

(63) Peng, Z.; Freunberger, S. A.; Hardwick, L. J.; Chen, Y.; Giordani, V.; Bardé, F.; Novák, P.; Graham, D.; Tarascon, J.-M.; Bruce, P. G. Oxygen Reactions in a Non-Aqueous Li⁺ Electrolyte. *Angew. Chem. Int. Ed.* **2011**, *50* (28), 6351-6355. <https://doi.org/10.1002/anie.201100879>.

- (64) Jia, M.; Li, H.; Qiao, Y.; Wang, L.; Cao, X.; Cabana, J.; Zhou, H. Elucidating Anionic Redox Chemistry in P3 Layered Cathode for Na-Ion Batteries. *ACS Appl. Mater. Interfaces* **2020**, *12* (34), 38249-38255. <https://doi.org/10.1021/acsami.0c11763>.
- (65) Yu, L.; Dong, H.; Chang, Y.-X.; Cheng, Z.; Xu, K.; Feng, Y.-H.; Si, D.; Zhu, X.; Liu, M.; Xiao, B.; et al. Elucidation of the sodium kinetics in layered P-type oxide cathodes. *Sci. China Chem.* **2022**, *65* (10), 2005-2014. <https://doi.org/10.1007/s11426-022-1364-1>.
- (66) Chagas, L. G.; Buchholz, D.; Vaalma, C.; Wu, L.; Passerini, S. P-type $\text{Na}_x\text{Ni}_{0.22}\text{Co}_{0.11}\text{Mn}_{0.66}\text{O}_2$ materials: linking synthesis with structure and electrochemical performance. *J. Mater. Chem. A* **2014**, *2* (47), 20263-20270, 10.1039/C4TA03946G. <https://doi.org/10.1039/C4TA03946G>.
- (67) Maddukuri, S.; Valerie, P.; Upadhyayula, V. V. Synthesis and Electrochemical Study of New P3 Type Layered $\text{Na}_{0.6}\text{Ni}_{0.25}\text{Mn}_{0.5}\text{Co}_{0.25}\text{O}_2$ for Sodium-Ion Batteries. *ChemistrySelect* **2017**, *2* (20), 5660-5666. <https://doi.org/10.1002/slct.201700376>.
- (68) Zhou, Y.-N.; Wang, P.-F.; Zhang, X.-D.; Huang, L.-B.; Wang, W.-P.; Yin, Y.-X.; Xu, S.; Guo, Y.-G. Air-Stable and High-Voltage Layered P3-Type Cathode for Sodium-Ion Full Battery. *ACS Appl. Mater. Interfaces* **2019**, *11* (27), 24184-24191. <https://doi.org/10.1021/acsami.9b07299>.
- (69) Zhao, S.; Yu, X.; Zhao, Y. A water-stable high-voltage P3-type cathode for sodium-ion batteries. *Chin. Chem. Lett.* **2024**, 109933. <https://doi.org/10.1016/j.ccllet.2024.109933>.
- (70) Liu, Y.; Liao, J.; Tang, Z.; Chao, Y.; Chen, W.; Wu, X.; Wu, W. Improved Sodium Storage Performance of Zn-Substituted P3- $\text{Na}_{0.67}\text{Ni}_{0.33}\text{Mn}_{0.67}\text{O}_2$ Cathode Materials for Sodium-Ion Batteries. *J. Electron. Mater.* **2023**, *52* (2), 864-876. <https://doi.org/10.1007/s11664-022-10045-7>.

- (71) Brahmanandan, S.; Nair, S.; Santhanagopalan, D. High-Performance Zr-Doped P3-Type $\text{Na}_{0.67}\text{Ni}_{0.33}\text{Mn}_{0.67}\text{O}_2$ Cathode for Na-Ion Battery Applications. *Crystals* **2023**, *13* (9), 1339. <https://www.mdpi.com/2073-4352/13/9/1339>.
- (72) Weppner, W.; Huggins, R. A. Determination of the Kinetic Parameters of Mixed-Conducting Electrodes and Application to the System Li_3Sb . *J. Electrochem. Soc.* **1977**, *124* (10), 1569. <https://doi.org/10.1149/1.2133112>.
- (73) Yoncheva, M.; Stoyanova, R.; Zhecheva, E.; Kuzmanova, E.; Sendova-Vassileva, M.; Nihtianova, D.; Carlier, D.; Guignard, M.; Delmas, C. Structure and reversible lithium intercalation in a new P'3-phase: $\text{Na}_{2/3}\text{Mn}_{1-y}\text{Fe}_y\text{O}_2$ ($y = 0, 1/3, 2/3$). *J. Mater. Chem.* **2012**, *22* (44), 23418-23427, 10.1039/C2JM35203F. <https://doi.org/10.1039/C2JM35203F>.
- (74) Jo, J. H.; Kim, H. J.; Choi, J. U.; Voronina, N.; Lee, K.-S.; Ihm, K.; Lee, H.-K.; Lim, H.-D.; Kim, H.; Jung, H.-G.; et al. Facilitating sustainable oxygen-redox chemistry for P3-type cathode materials for sodium-ion batteries. *Energy Storage Mater.* **2022**, *46*, 329-343. <https://doi.org/10.1016/j.ensm.2022.01.028>.



TOC graphic

Supporting Information

Elucidating the Electrochemical Behaviour of a P3-type High Na Content Cathode

Samriddhi Saxena^a, Manish Badole^a, Hari Narayanan Vasavan^a, Velaga Srihari^b, Asish Kumar Das^a, Pratiksha Gami^a, Neha Dagar^a, Sonia Deswal^c, Pradeep Kumar^c, Himanshu Kumar Poswal^b, Sunil Kumar^{a,*}

^a *Department of Metallurgical Engineering and Materials Science, Indian Institute of Technology Indore, Simrol, 453552, India*

^b *High Pressure & Synchrotron Radiation Physics Division, Bhabha Atomic Research Centre, Mumbai, 400085, India*

^c *School of Physical Sciences, Indian Institute of Technology Mandi, Mandi, 175005, India*

*E-mail: sunil@iiti.ac.in

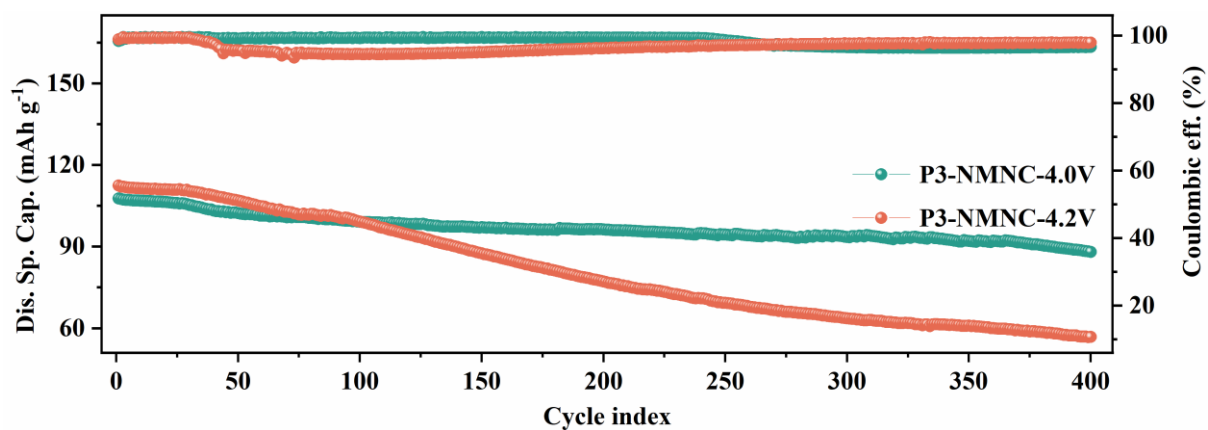


Figure S1. Cycle performance of P3-NMNC at 3C.

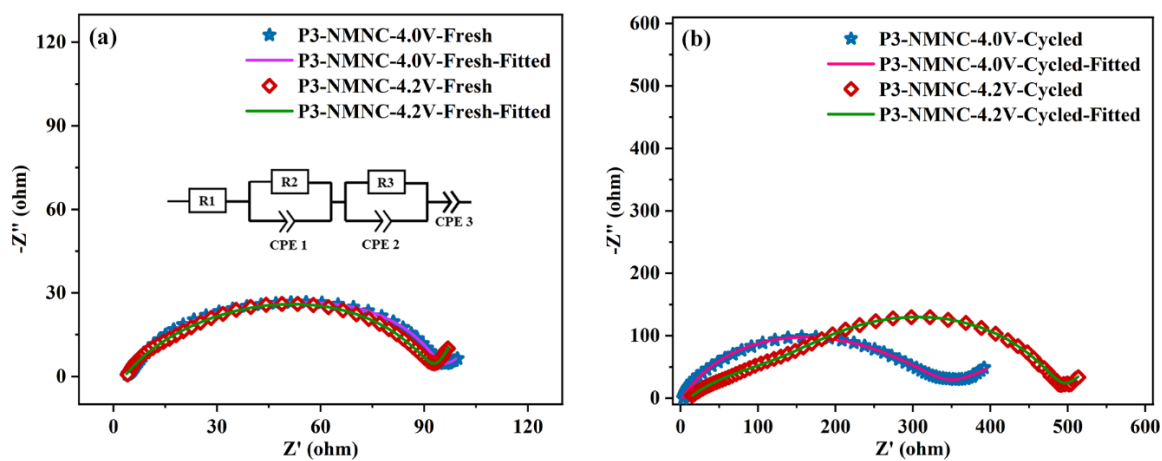


Figure S2. The Nyquist plots for (a) fresh half-cells with P3-NMNC cathode (b) half-cells with P3-NMNC cathode cycled (400 cycles at 3C) in different voltage ranges. Inset S2(a) shows the equivalent circuit used for fitting.